ADVANCED FUNCTIONAL MATERIALS
www.afm-journal.de

Programmable Entanglement of Granular Mechanical Metamaterials

*Ashkan Rezanejad, Mostafa Mousa, Christian D. Lorenz, Matthew Howard, and Antonio Elia Forte**

Entanglement between objects offers a powerful route to programmable collective behavior in granular media. Here, the concept of entangled granular metamaterials—clusters of geometrically complex grains is introduced, whose interlocking interactions drive emergent and tunable properties. The geometric features that promote entanglement are identified, distinguished from simple contact interactions, and the strength of entanglement is quantified through disentanglement dynamics. By varying the number and shape of grains, the degree of interlocking within the cluster is modulated, and its utility is demonstrated in robotic handling tasks. Using a ferromagnetic grain assembly manipulated by an electromagnet, the metamaterial is deployed onto a second, non-ferromagnetic cluster of complex targets. The grains penetrate and entangle with the targets, enabling robust collective picking and even selective retrieval of individual objects with intricate geometry. Finally, strategies for controlled separation of the grains from the targets are outlined, establishing a foundation for programmable entanglement in matter manipulation.

1. Introduction

Materials made of "grains" have shown interesting functionalities, resulting in adaptive,[1] programmable,[2] and jamming[3] granular media, which have been used to design devices for impact mitigation, energy absorption, and robotic gripping, respectively. Different grain shapes, such as beams,[4] rods[5] or ellipsoids,[6,7] further influence the properties of these materials. For instance, birds' nests are a natural example of structures made from beam-shaped grains.[8]

Mechanical metamaterials have emerged as a design platform to engineer material properties that depend on the material's structure rather than its composition.[9–12] Examples of these are metamaterials that can manipulate light,[13] surface roughness,[14] radio frequencies,[15] and dynamic responses.[16]

In most cases, mechanical metamaterials are continuous and characterized by a repeating pattern, which enables the design of novel actuators,[17] robotic grippers,[18] and solar panels.[19] However, there also exist disordered metamaterials with non-repeating patterns that occur naturally and offer enhanced properties—for example, the superior toughness found in animal bones.[20–23] Taking this concept further, disordered metamaterials can consist of disconnected elements, with individual cells functioning like grains. Interestingly, if the grains are designed to be geometrically complex, collective behaviors emerge from the granular media. Such systems are referred to as "granular metamaterials",[2,24,25] where the grains exhibit a high degree of interaction in confined environments (e.g., granular viscosity).

Entanglement is a special type of interaction that occurs when objects (or grains) have a propensity to interlock due to their peculiar shape.[26,27] For instance, it has been demonstrated that entangled grains can be used for architectural structures.[28] While spiky objects are naturally inclined to entangle, longer spikes tend to reinforce separation.[29]

Recent strategies have exploited entanglement to achieve functionality in robotic picking and grasping rigid and (mainly) singular objects.[30,31] Despite the wide range of gripper designs available,[32] entangled objects remain exceptionally difficult to pick consistently using conventional robotic grippers, including parallel grippers, 3-finger or anthropomorphic hands, and scoops.[33–36]

Here, we identify geometrical features that cause entanglement, driving the grains to behave collectively. To gain a better understanding of entanglement, we design a family of grains with varying degrees of geometrical complexity and test how they interact with each other. To measure the number of entangled interactions, we create a set of criteria that, if met, ensures some level of entanglement between two grains. We then assess the strength of such entanglement via molecular dynamics simulations.

Next, we hypothesize that a cluster formed by grains with a high propensity to entangle will also show a high propensity to interact with a second cluster of entangled objects. We therefore present a novel strategy that employs magnetic stimuli to

A. Rezanejad, M. Mousa, C. D. Lorenz, M. Howard, A. E. Forte
Department of Engineering
King's College London
London WC2R 2LS, UK
E-mail: antonio.forte@kcl.ac.uk, antonio.forte@eng.ox.ac.uk

The ORCID identification number(s) for the author(s) of this article can be found under https://doi.org/10.1002/adfm.202516484

DOI: 10.1002/adfm.202516484

manipulate a granular metamaterial, which entangles and picks tangle-prone objects, such as woollen yarns, herbs, and nettings, with relatively high consistency.

Additionally, we demonstrate the effectiveness of our method to pick single objects with complex geometries and present manufacturing strategies to create decomposable grains, which leads to entanglement deactivation and separation of the targets from the metamaterial. Thus, by reducing the robotic control parameters to a minimum and harnessing the flexibility of metamaterial design, our method opens new pathways for robotic gripping and manipulation, simplifying operations and embedding functionality into the hardware.

2. Results and Discussion

2.1. Emergence of Global Behavior in Granular Media

The mechanical behavior of granular materials arises from the characteristics of individual grains and the physical interactions occurring between them. The complexity of these interactions varies depending on the grains' material properties and geometrical features, as well as the environmental conditions.[24–28] Among these factors, geometrical features of grains result in a distinct type of interaction, which can be classified as entanglement. For instance, recent studies show that the degree of entangled interaction in a cluster of U-shaped grains is influenced by the aspect ratio of their geometric parameters (length, width, and angle).[29,37] However, rather than fine-tuning these parameters to control the system's collective behavior, here we explore the geometrical complexity of grains—which increases with the number of corners per grain (N_c). This allows greater flexibility in programming material behavior.

We introduce a simple design method to create grains with increasing geometric complexity. To this end, we present an algorithm to design grains ranging from 0 to 4 corners (see **Figure 1A**). The algorithm follows five rules for constructing a grain made of segments: 1) the building block is a segment, which has a complexity order of zero, with a start and an end point; 2) in order to increase complexity, a new segment is attached to an end point of the previous segment; 3) each successive segment is perpendicular to the preceding one, while remaining within the same plane; 4) the orientation of each new segment is chosen to minimize the rectangular area of the grain's bounding box; and 5) grains cannot form enclosed shapes. This structured approach allows us to systematically create grains with varying levels of complexity for our experiments.

2.1.1. The Role of Grain Geometry in Packing Efficiency and Entanglement Formation

Once we have designed our grain types, we measure the packing fraction of grains with different geometrical complexities. To do this, we run molecular dynamics (MD) simulations (using LAMMPS),[38] which we then validate against physical experiments (see Figure 1B). The experimental setup consists of a cylindrical container (diameter 50 mm, height 100 mm) filled with homogeneous rigid grains (laser-cut acrylic, see Section S1, Supporting Information). The number of grains is set so that the container is filled with the same number of segments (i.e., 800 segments) across different grain types (e.g., grain type 4 contains 5 segments, therefore 160 grains are used). The grains are poured into the container and vibrated for 10 s (using a custom-made vibration rig, refer to Section S1, Supporting Information) to enhance interactions and compact the granular media. We then measure the height of the granular structure inside the container (G_h). In simulations, this is calculated by doubling the z-coordinate of the center of mass, ensuring a consistent measurement approach.[29] For more details of the granular MD simulations, refer to Section S2 (Supporting Information). We then calculate the packing fraction ($P.F.$) as the ratio of the volume occupied by the grains (V_g–constant across grain types, as the total number of segments is the same) to the volume of the structure inside the container (V_c–differs for each grain type, as this is based on the height of the granular structure that emerges, G_h). Furthermore, we repeat this experiment with other rigid grains made from wood and steel (refer to Section S1, Supporting Information). We show that, for the small masses used in our setup, variations in surface friction (coefficient range = [0.3–0.6]) and density (range = [0.9–7.5] g cm^{-3}) do not notably influence the granular packing fraction for the same grain type (see Figure 1C). However, it is clear that geometrical complexity (i.e., the number of corners in our system–N_c) dictates how the grains pack together (governed by an exponential law: $P.F. = 0.31e^{-0.43N_c}$).

Additionally, we use MD simulations to investigate the effect of the number of grains (granular mass) on the packing fraction (see Figure 1D). The results indicate that, although there is a notable increase in packing fraction between 1 and 5 g of granular mass, this plateaus beyond a certain threshold (above 20 g). We attribute this behavior to a tendency to compact, and we notice that grains with lower complexity exhibit a higher propensity to compact as the granular mass in the container increases. This results in a significant variation of packing fraction (e.g., over 60% for $Nc = 0$). Conversely, grains with higher complexity show resistance to compacting, which indicates that their packing behavior is significantly less dependent on granular mass (e.g., less than 5% for $Nc = 4$).

Moreover, we explore the impact of container size relative to grain size. Due to the cylindrical shape of the container, we first identify the smallest circular area that each grain can fit into and define its diameter as the grain diameter (d_g, see Figure 1E). We then determine the diameter of the cylindrical container (d_c) relative to the grain diameters (range d_c/d_g = [2–6]). The results indicate that for $d_c/d_g \geq 5$ the packing fraction remains unaffected by container size across all grain types (see Figure 1F).

Therefore, with a sufficiently large container and adequate granular mass, the primary factor influencing the packing fraction of rigid grains is their geometrical complexity. This complexity leads to entanglement, occurring when a grain's corner interlocks with another grain's corner or its adjacent segments. However, not every interaction between corners results in entanglement. Hence, one needs a set of rules to assess if two (or more) grains are entangled with each other.

A grain's corner has two adjacent segments which, if connected, form a triangle (Figure 1G (bottom)). Using such imaginary triangles, we hypothesize three criteria, which must all be satisfied for entanglement to occur: 1) a triangle must intersect

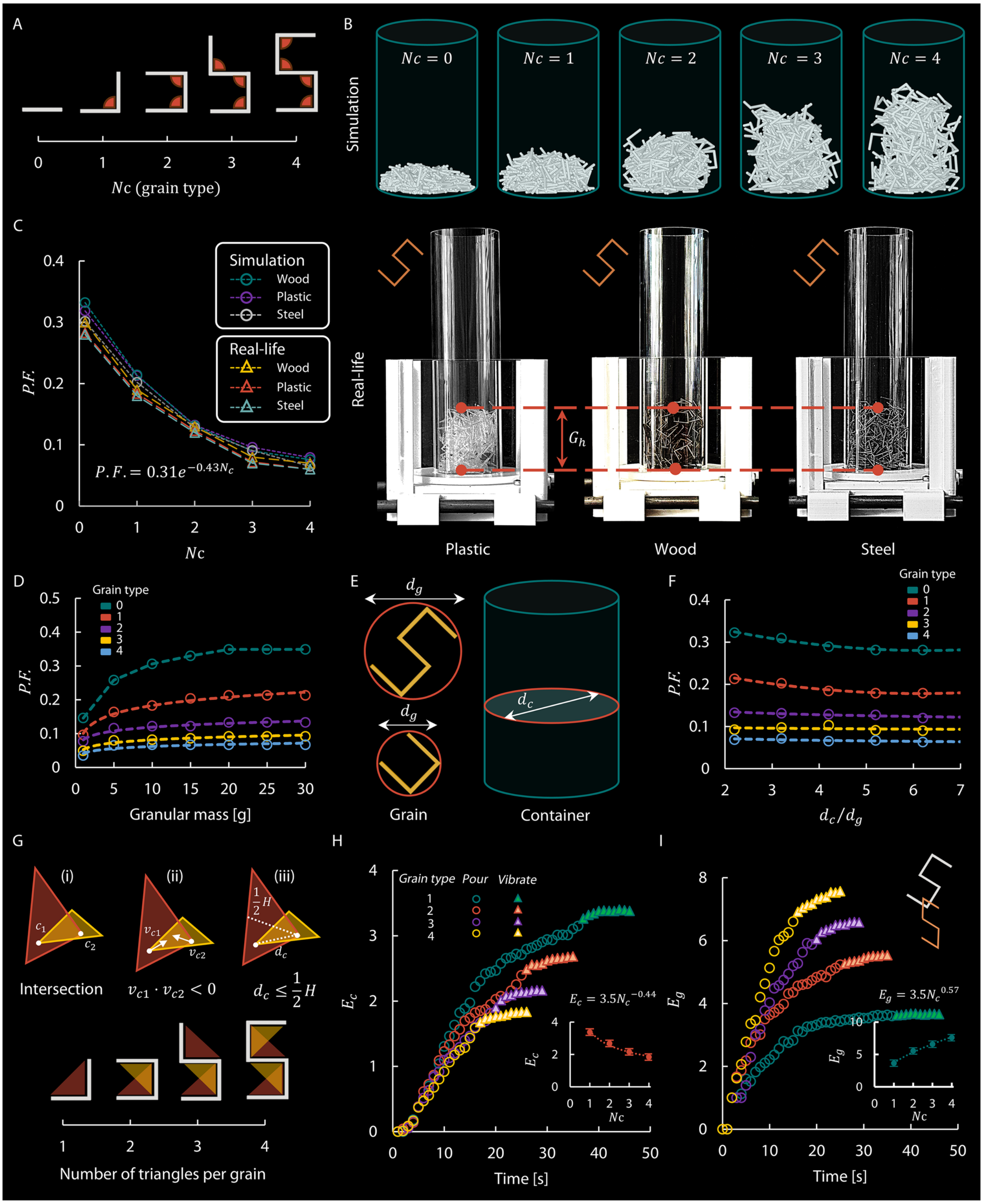

Figure 1. Emergence of collective behavior due to the grain's geometrical complexity. A) Evolution of the grain's geometrical complexity by increasing the number of corners. B) Packed granular clusters simulated in LAMMPS[38] (top), examples of real-life packed clusters with grain type 4 made of three different materials (bottom). C) Packing fraction of grains with different material properties, from both simulation and real-life experiments. D) The effect of granular mass on packing fraction. E) Illustrations of grain and container diameters. F) The effect of container size on granular packing fraction. G) Entanglement criteria (top), number of triangles created for each grain type (bottom). H) Average number of tangled corners per one corner over time (includes poring and vibration); the mean of the average entanglement per corner during vibration with standard error for each grain type (inlet). I) Average number of tangled grains per one grain over time (includes poring and vibration); the mean of the average entanglement per grain during vibration with standard error for each grain type (inlet), the legend is shared with panel H.

with another triangle (Figure 1G (i)); 2) the bisector vectors of the corners (i.e., 90° angle of the triangle) must have a negative dot product, meaning that they face each other (Figure 1G (ii)); and 3) the Euclidean distance between the two corners must be less than half the hypotenuse of the imaginary triangle, which we hypothesize to be sufficiently close to create entanglement (Figure 1G (iii)). It is worth noticing that these criteria are applicable to both homogeneous and mixed clusters of grain types (e.g., 50% grain type 2 and 50% grain type 3). However, in this work, we focus on investigating the behavior of homogeneous clusters of grains and distinguishing their unique entanglement behavior.

To this end, we use MD-simulated samples with a total mass of 20 g, placed in a container whose diameter is five times that of the grains. The grains are poured into the container and then subjected to vibration for 10 s. For every grain in the cluster, we measure: 1) the number of external corners entangled with each of its corners; and 2) the total number of grains entangled with it. Using these measurements, we calculate the average number of entangled corners per corner (E_c) and the average number of entangled grains per grain (E_g). The results show that, when looking at individual corners, the degree of entanglement per corner decreases for higher grain complexity (see Figure 1H). For example, in grain type 1, each corner entangles on average with ≈3.5 other corners. Instead, the corners of grain type 4 tangle on average with ≈1.8 other corners (governed by a negative power law: $E_c = 3.5 N_c^{-0.44}$). However, when looking at individual grains, more complex shapes entangle with more grains than simpler ones, as they have more corners at their disposal (governed by a positive power law: $E_g = 3.5 N_c^{0.57}$, see Figure 1I).

2.1.2. *Quantifying Entanglement Strength Through Escape Dynamics*

Our previous results showed that all grain types—except for grain type 0, which lacks corners and thus does not meet the entanglement criteria—exhibit entanglement that increases with geometric complexity. However, more complex grains tend to have lower packing fractions. As our current definition of entanglement is purely geometrical and does not account for interaction strength, we now aim to quantify the entanglement strength—that is, the tendency of grains to remain entangled—for each grain type.

To this end, we design a simulation to measure the propensity of each grain type to disentangle from its cluster (for further details, refer to Section S2, Supporting Information). Our hypothesis is that grains with lower complexity, despite being highly packed, show weaker entanglement strength. In our simulation, the grains are placed in an hourglass-shaped container. The container has a cylindrical upper and lower section (diameter $d_c = 5 d_g$) connected by a smaller cylindrical funnel (diameter d_h). The simulation involves pouring the grains in the upper part of the hourglass, then opening the funnel and vibrating the whole container for 10 s. This configuration allows us to measure the granular escape rate—the number of grains passing through the funnel per second (i.e., $E.R. = N_{eg}/t$, where N_{eg} is the number of escaped grains and t is time)—which serves as an indicator of entanglement strength. To reach a constant escape rate for every grain type, we sweep the funnel diameter with respect to the grain diameter ($d_h = [2, 2.5, 3, 3.5, 4] \times d_g$). As a criterion, we consider the escape rate as "constant" when N_{eg}/t can be fitted with a linear regression with $R^2 \geq 0.95$. Since the grains vary in size, maintaining a constant escape rate ensures consistent environmental conditions across all grain types. We report the escape rates and select the smallest funnel diameter that yields a constant escape rate (see **Figure 2A**).

Screenshots of the simulation for each grain type with the selected funnel hole d_h are shown in Figure 2B. Additionally, the number of grains that escape over time for the selected cases is reported in Figure 2C.

Notably, higher geometrical complexity means higher entanglement strength, as we measure ≈400 grain type 0, against ≈20 grain type 4 passing through the hole in the span of 10 s. Figure 1D shows the escape rate as a function of the number of corners in the grains, which demonstrates a decreasing exponential trend ($E.R. = 32.95 e^{-0.61 N_c}$) as complexity increases.

To predict the entanglement strength of any granular medium, we present our findings in a generalized format: we plot the escape flux ($\varphi = 4 \frac{E.R.}{\pi {d_h}^2}$, i.e., $E.R.$ normalized by the funnel hole area) against the packing fraction (see Figure 2E), which is a characteristic of each grain type as shown by the results in Figure 1. We conclude that granular media with higher packing fractions exhibit higher escape fluxes, which correspond to lower levels of entanglement. Hence, packing fraction can be used as a direct indicator of disentanglement flux, with a power law that links the two variables ($\varphi = 1.13 * P.F.^{2.43}$).

The result from these simulations supports our previous findings, demonstrating that even in dynamic scenarios, grains with a higher geometrical complexity exhibit greater levels of entanglement. As this is a global, emerging behavior that arises purely from the interactions between geometrically complex grains, we define such a medium "entangled granular metamaterial". Notably, this terminology has since been adopted by recent studies,[37] following its initial introduction in the preprint version of our current work.[39]

2.2. Tangled Picking

We now leverage the granular metamaterials' propensity to self-entangle to create a momentary structure that can also entangle with a secondary cluster of targets. Such a secondary cluster is made of objects that are elongated and flexible, in order to simulate real-life objects that are prone to tangle (e.g., fresh herbs and woollen yarn). We then harness the entanglement between the grains and the targets to perform a picking task. To manipulate the grains easily, we use ferromagnetic grains (made of steel) to can be dropped and retrieved with an electromagnet. We test this method in a simulated environment and with real-life experiments.

We design two target shapes, each with a length of 100 mm and a thickness of 1 mm: 1) non-spiky (e.g., woollen yarn) and 2) spiky ones (e.g., fresh herbs). The target's geometrical parameters are determined based on a real-life pilot study conducted to evaluate the effects of targets' length, thickness, and spikiness on entangled picking. The results of this study reveal that the target's length and thickness significantly influence its propensity to entangle. In particular, longer and thinner targets show higher

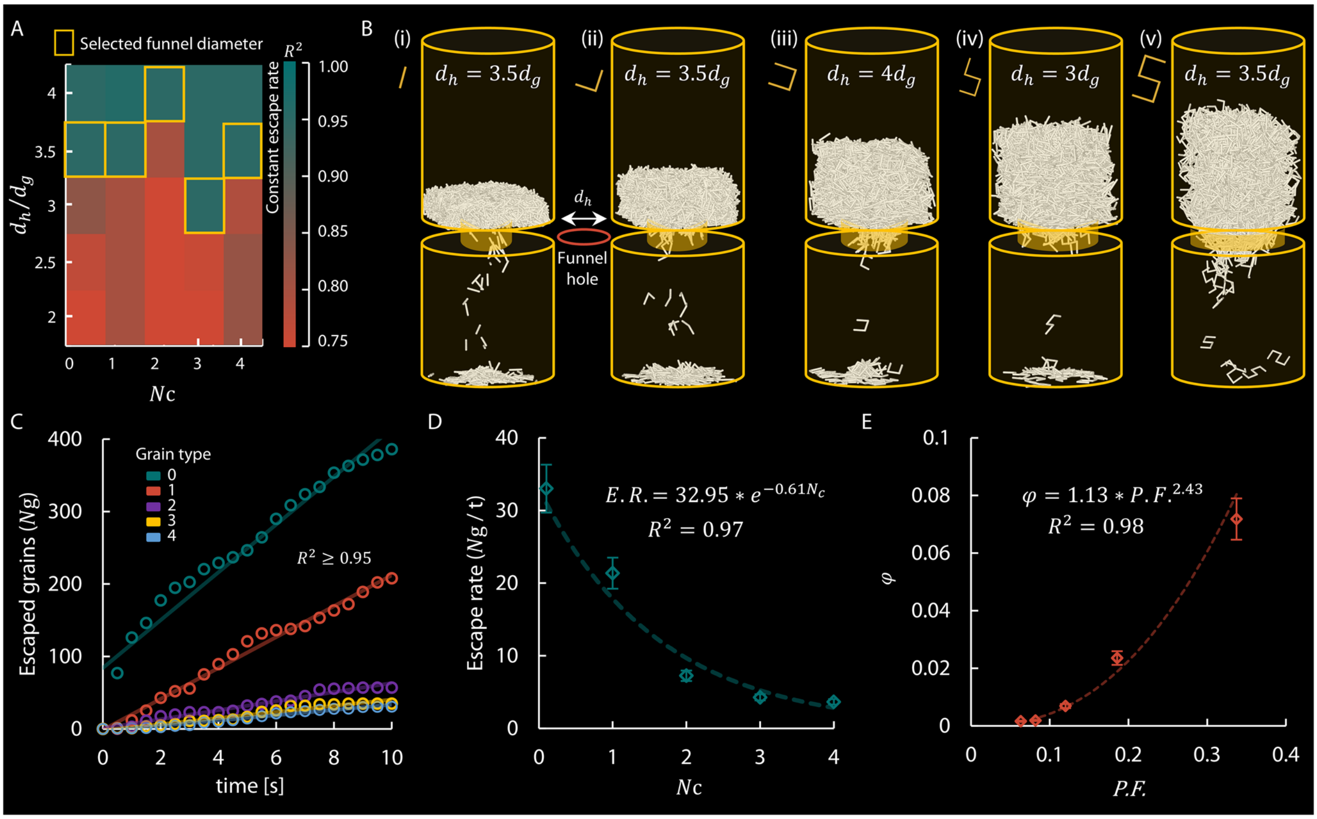

Figure 2. Disentanglement of granular clusters. A) The R^2 value obtained when one fits the number of grains that escape over time with a linear regression, for different ratios of funnel diameter with respect to the grain diameter across grain types. B) The snapshot of the hourglass simulation with the selected funnel diameters. C) The number of escaped grains over time for each grain type (through the selected funnel diameters). D) The escape rate for each grain type with an exponential trendline. E) The escape flux as a function of packing fraction and its governing power law.

entanglement (for further details, please refer to Section S3, Supporting Information). Therefore, we fix the length and thickness of the targets to solely focus on the geometrical features of the grains. This setup allows us to analyze how different grain types interact with entangled targets.

2.2.1. MD Simulation of Tangled Picking

In the simulation, the picking task is as follows: first, we pour the targets (deformable and non-ferromagnetic) into a cylindrical container (diameter = 100 mm). Then we shake the container for 10 s to create a randomized topology. Afterward, we pour the grains (rigid and ferromagnetic) with random positions and orientations on top of the targets to initiate interaction. We then simulate the approach of an electromagnet, modelled as a cylindrical disk, toward the cluster. The electromagnet stops upon making full contact with the cluster. Once activated, it applies an upward vertical force exclusively to the grains, effectively retrieving them along with a portion of the targets entangled to them (see **Figure 3A**). We perform 10 replica simulations of each system and record the mean and standard deviation. We use these simulations to investigate the effect of four parameters: i) grain type (N_c = [0, 1, 2, 3,4]); ii) target type(i.e., spiky and non-spiky); iii) number of targets (N_t = [50, 100, 150, 200]) and iv) number of deployed grains (N_g = [50, 100, 150, 200]). For details on the entangled picking simulation, refer to Section S4 (Supporting Information).

The results, presented in Figure 3B, reveal a higher picking ratio (i.e., picked targets over the number of targets, $\frac{Pick}{N_t}$) for grains with higher complexity. This can be attributed to a higher propensity for entanglement in such grains, which aligns with prior findings. Moreover, the picking ratio decreases as the total number of targets increases, suggesting that the number of picked targets is dependent on the number of targets in the container (for a comparison between *Pick* and N_t, refer to Section S5, Supporting Information). Additionally, deploying a larger quantity of grains leads to more targets being picked, as the increased number of grains enhances opportunities for entanglement. Lastly, in most cases (except for N_t = 50), spiky targets exhibit a slightly higher picking ratio in comparison to non-spiky ones, demonstrating that spiky targets are more prone to entanglement.

2.2.2. Real-Life Tangled Picking

To verify the simulation results, we design an experimental setup comprising a robotic arm, an electromagnet mounted on the robotic end-effector, ferromagnetic grains, a cluster of targets in a container, and a vacuum generator with a transparent container

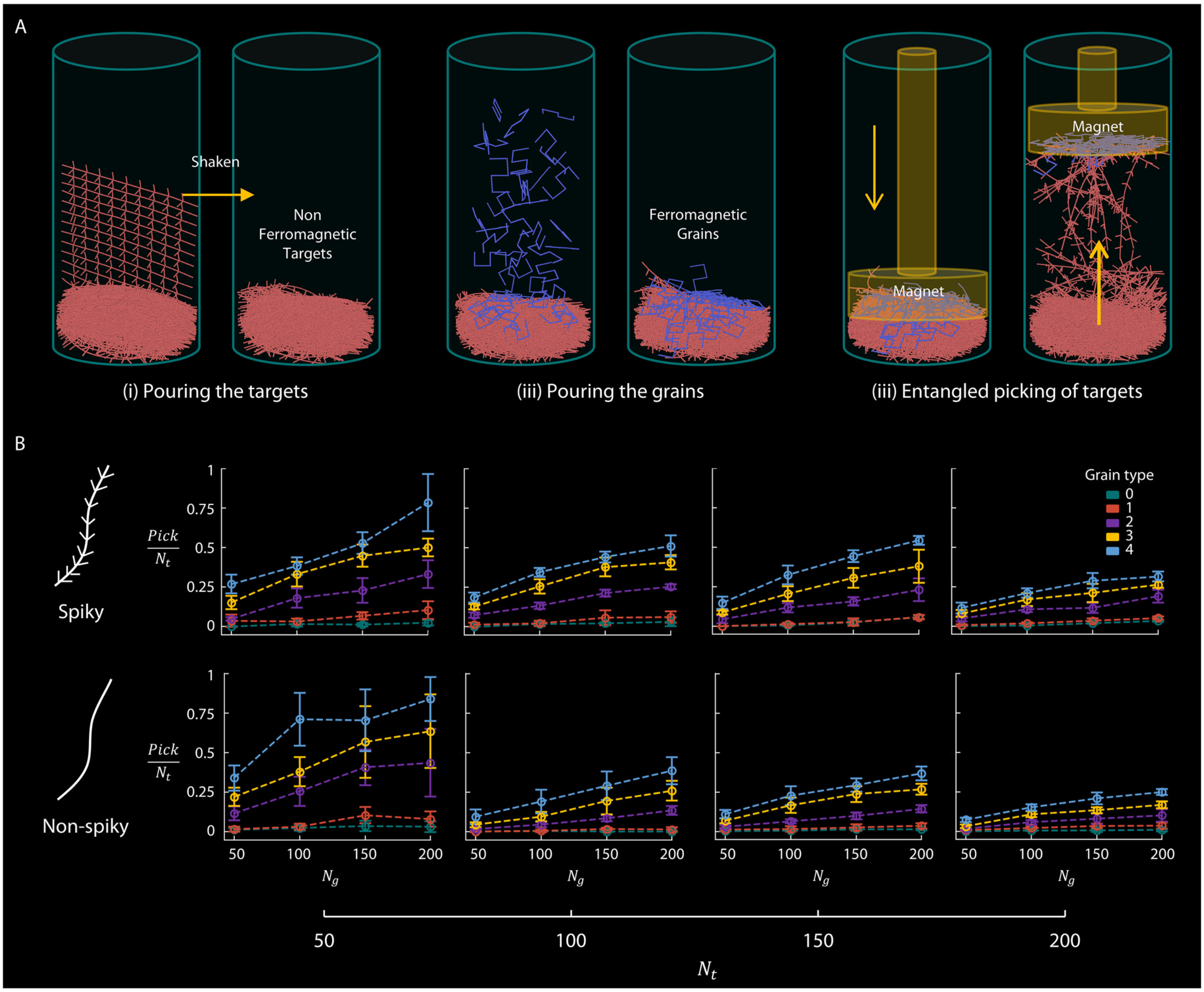

Figure 3. Simulated tangled picking. A) Snapshots of the three steps in the tangled picking simulation (for the case: N_t = 200, spiky targets, N_g = 50, and grain type 4). B) The picking ratio (*Pick*/ N_t, mean and standard deviation) across varying numbers of targets (N_t), number of deployed grains (N_g), grain type, and target type.

(see **Figure** 4A (i)). For more information about the devices used in the experimental setup, refer to Section S6, Supporting Information.

The experimental procedure begins with the robotic arm approaching a container filled with ferromagnetic grains and picking them up by activating an electromagnet mounted on its end-effector (Figure 4A (ii)). The robotic arm then moves its end-effector above the targets and deactivates the electromagnet, resulting in a sudden drop of all the picked grains onto the cluster of entangled targets (Figure 4A (iii)). The grains penetrate the cluster and create entanglement. Afterward, the robotic arm approaches the targets and reactivates the electromagnet to attract all the grains once again. This results in the picking of both the grains and the targets, as they are entangled together (Figure 4A (iv)). Lastly, the picked entangled media are moved to the opening of the vacuum suction duct, which pulls the targets away from the grains held by the electromagnet (Figure 4A (v)). The separated targets are then transferred into a transparent enclosed container under the vacuum generator (Figure 4A (vi)). It's important to note that relying solely on vacuum suction as a gripper does not allow for consistent control over the quantity picked.

We conducted 10 iterations of the experiment for each grain type (N_c = [2, 4]) and the number of deployed grains (N_g = [50100150]). Additionally, we selected two real-life targets with geometrical characteristics similar to those of the simulated ones. For spiky targets, we use fresh parsley, with each stem weighing ≈0.4 g, and lengths varying from ≈50 to ≈150 mm, and thicknesses ranging from ≈0.8 to ≈2.2 mm. For non-spiky targets, we use woollen yarns with a diameter of 1 mm and cut to a length of 100 mm.

The real-life picking of both spiky and non-spiky targets closely aligns with the simulated data, demonstrating a consistent increase in the picking ratio as the number of deployed grains increases. Furthermore, grains with complex shapes outperform

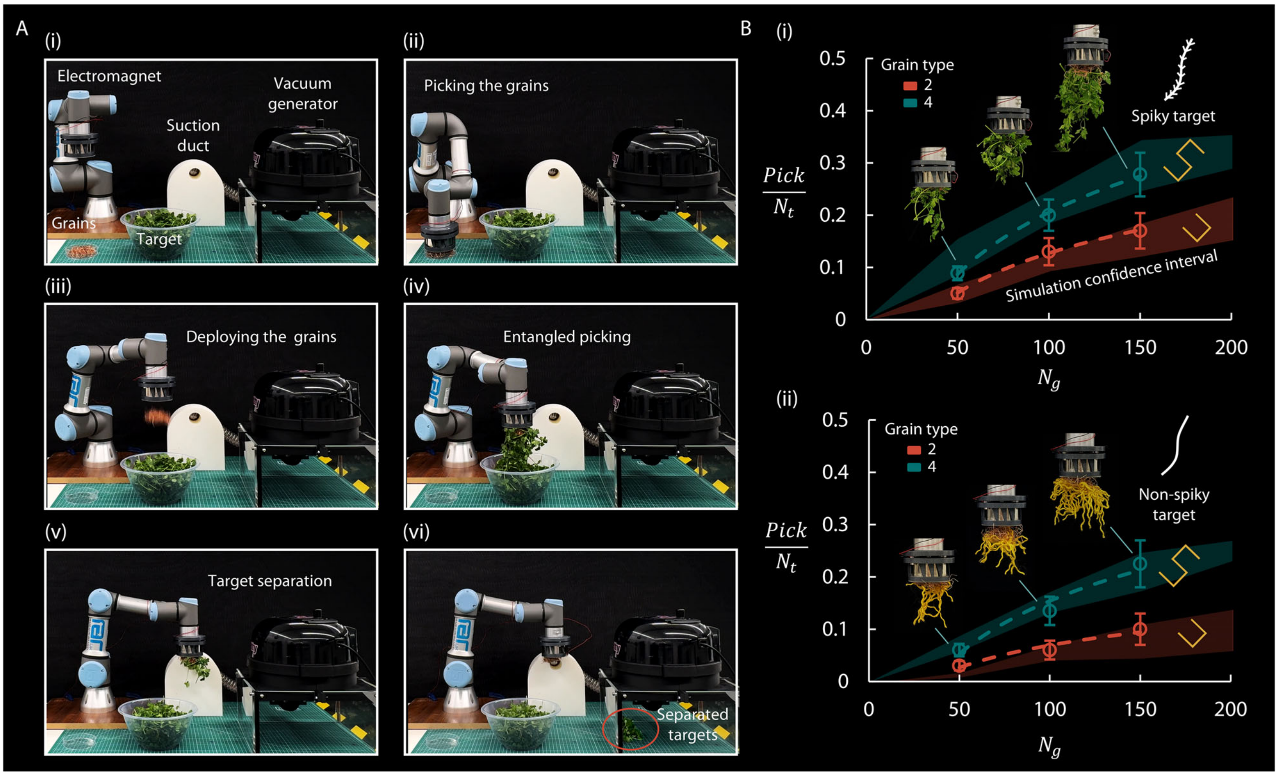

Figure 4. Real-life tangled picking. A) Step-by-step picking process of our robotic grasping approach. B) The picking ratio of (i) spiky and (ii) non-spiky targets with two different grain types and a varying number of deployed grains. The markers and error bars represent the average and standard deviation of the real-life picking results. The highlighted confidence intervals correspond to the simulation data, with the upper and lower limits reflecting their standard deviation.

less complex ones during the picking task (see Figure 4B). Notably, similar to the simulation, spiky targets exhibit a higher picking ratio compared to non-spiky ones, due to their greater propensity for tangling.

2.2.3. Picking and Sorting Tangle-Prone Objects

Next, we qualitatively demonstrate the picking of various objects categorized as "tangle-prone" (see **Figure** 5A). These objects are grouped into two classes: rigid and deformable. For the rigid ones, we identify two subclasses: perforated objects (e.g., crates and wheels), and clawed objects (e.g., hair combs and hair claw clippers). Similarly, we identify two subclasses for the deformable category: netting (e.g., fishing nets and net bags) and elongated deformable clusters (targets previously investigated in Figure 4). We pick each of these objects 10 times with two different grain types (N_c = 2 and 4, N_g = 100), measure the success rate (successful picks out of 10 tries), and report the mean results (for objects of the same subclass) in Figure 5B.

Grain type 4 shows a higher success rate for all subclasses (≥80%), while type 2 is less performant (≥60%). Notably, nettings are more tangle-prone, as they exhibit the highest success rate for both grain types, whereas clawed objects are more difficult to pick, as they tend to slide out of the cluster of grains, due to the openings of their claws.

Additionally, we demonstrate sorting items into "tangle-prone" and "non-tangle-prone" categories through picking. For this, a conveyor belt is used to transfer three objects in random order to the picking workspace (see Figure 5C (i)). The robotic end-effector deploys grains onto each object as it enters the workspace and attempts to pick them. Predictably, the robot fails to pick the two non-perforated objects, so they travel to the end of the conveyor and fall into bin 1, as no entanglement between the grains and the target occurs (see Figure 5C (ii,iii)). However, it successfully picks the perforated object which entangled with the deployed grains (see Figure 5C (iv)) and places it into bin 2. This shows our ability to pick and sort objects that belong to different categories with minimal control.

2.2.4. Design and Testing of Decomposable Grains

Lastly, we demonstrate two types of decomposable grains (see Figure 5D) to attain complete release of the picked target by dismantling or melting the grains instead of separation by vacuum suction (refer to Section S7, Supporting Information for details of fabrication).

The first type (FWD, i.e., ferromagnetic water dismantlable) is constructed from a water-soluble casing and ferromagnetic steel bars. The casing is 3D printed using BVOH (Butenediol vinyl alcohol co-polymer, Ultrafuse BVOH, BASF) due to its ability to dissolve in water. The steel bars are firmly fitted and secured in

ADVANCED FUNCTIONAL MATERIALS
www.afm-journal.de

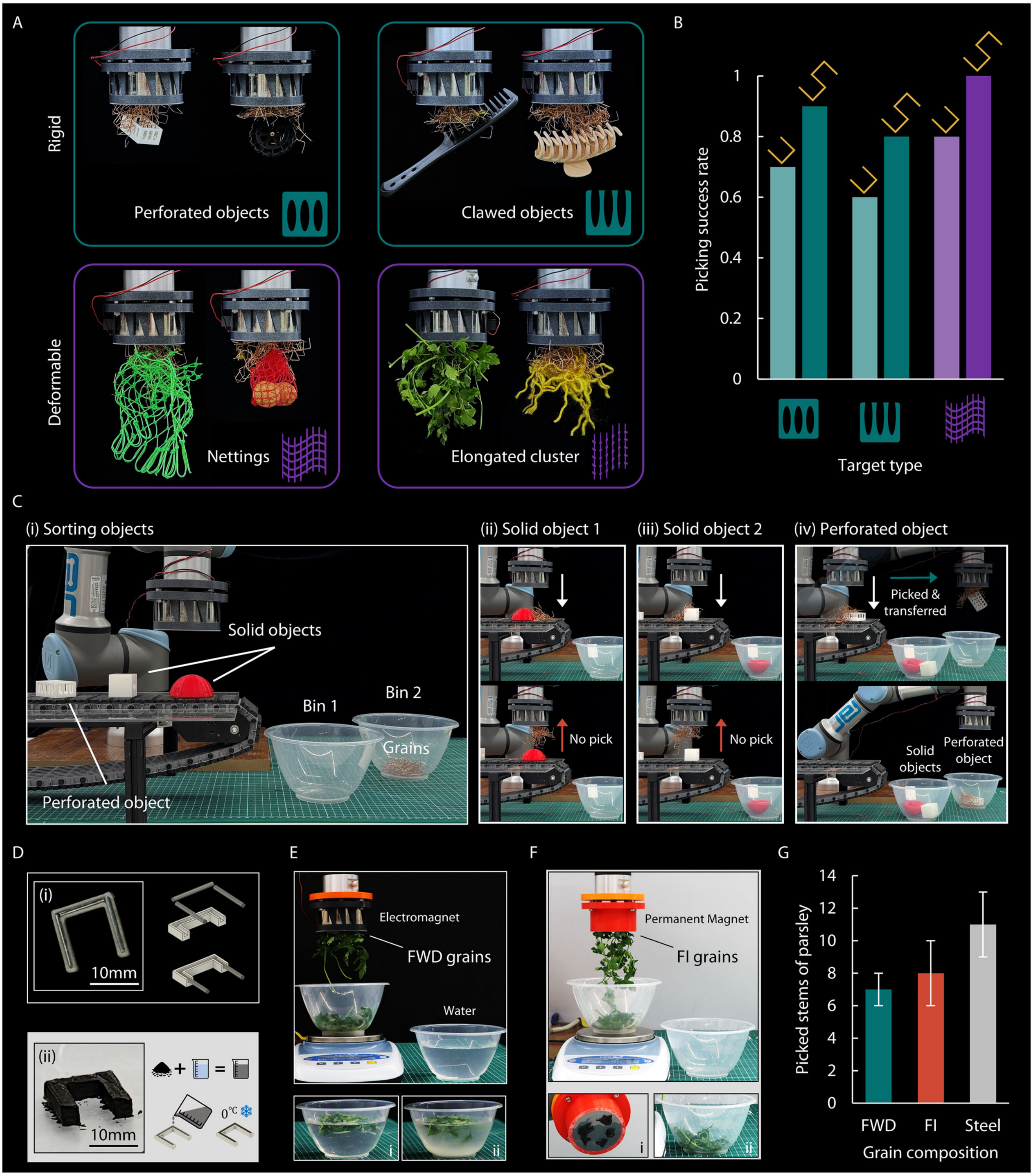

Figure 5. Picking/sorting tangle-prone objects and testing decomposable grains. A) Entangled picking of rigid and deformable objects. B) The mean picking success rate of perforated objects, clawed objects, and nettings. C) The sorting process of a perforated object from solid objects. D) Ferromagnetic water dismantlable (FWD) grains constructed from steel bars and 3D printed BVOH casing (top); ferromagnetic ice (FI) grains constructed from water and ferromagnetic iron oxide powder (bottom). E) Picking fresh parsley using an electromagnet and ferromagnetic dismantlable grains; targets and grains are dropped into water (i); the BVOH casing of the grains dissolves when in water, resulting in dismantling and sinking of the metal bars (ii). F) Picking fresh parsley using a permanent magnet and ferromagnetic ice grains; the remaining ferromagnetic powder collected on the magnet after the grains are melted (i); the targets are released in the dropping zone (ii). G) The mean and standard deviation of picked fresh parsley using the two types of decomposable grains and steel grains (grain type 2, $N_g = 25$, $N_t = 25$).

ADVANCED FUNCTIONAL MATERIALS
www.afm-journal.de

the casing, and the picking experiment is run. The picked media is then dropped in water. When the constructed grains come into contact with water, the casing disintegrates, and the metal bars are released. Due to their shape and density, the short metal bars are prone to getting tangled with the targets and sinking in the water (see Figure 5E).

The second proposed design (FI, i.e., ferromagnetic ice) is fabricated by mixing water with food-safe ferromagnetic powder (commercially known as "black iron oxide" with the chemical composition of Fe_3O_4, EU food number: E172, The Crafters Shop, UK) in a ratio of 2 to 1 by weight. The liquid mixture is poured into a molding case and then placed inside a freezer to produce ferromagnetic ice as grains. An additional advantage is that this type of grain does not necessarily require an electromagnet, since the quick melting time (less than 2 min at room temperature) causes the grains to disintegrate, resulting in the release of the picked targets. To demonstrate this, we replace the electromagnet with a neodymium magnet (RS components), with a pull force of ≈400 N. This reduces the set-up cost, minimizes the control parameters, and allows for the iron oxide to be collected on the magnet and reused to create new grains (see Figure 5F).

The results reported in Figure 5G show a comparison between the picked stems of fresh parsley by the two decomposable grain types and the previously used steel grains (10 iterations, N_t = 25, N_g = 25). Both decomposable grain types pick around 7 and 8 stems of parsley, which is only ≈23% lower than the average picked amount obtained when using the steel grains.

3. Conclusion

The properties of mechanical metamaterials are typically deterministic, governed by the geometrical features of their permanently connected unit cells. In contrast, granular metamaterials rely on interactions between grains that do not require permanent attachment. This unique characteristic enables the material to be repeatedly decomposed and reassembled (i.e., reconfigured). While this introduces a degree of unpredictability to the system's behavior, it also allows for global control with a certain level of confidence when the grains interact within a cluster.

In this study, we demonstrated that by understanding how simple geometric features influence the fundamental packing behavior of grains—specifically their packing fraction, entanglement characteristics, and escape dynamics—we can predict the collective behavior of granular clusters when interacting with external forces, environments, or other objects. In particular, we investigated entanglement as a function of the geometrical complexity of grains, predicting that more complex grains would exhibit higher levels of entanglement based on geometric analysis and MD simulations (see Figure 1). To validate this prediction, we designed two experiments: i) disentangling grains from one another through escape dynamics (see Figure 2), and ii) entangling grains with external objects (see Figure 3). This study, therefore, extends beyond a purely empirical approach by integrating geometric methodologies to deepen the understanding of the underlying physical phenomena, which are subsequently validated through targeted experimentation.

The results of the disentangling experiment (see Figure 2) reveal a direct relationship between the funnel diameter of the hourglass and the rate at which untangled grains escape (fall through the funnel) from a homogeneous group. Notably, for each grain type, the escape rate becomes constant beyond a certain funnel diameter. By selecting these diameters, we can effectively normalize the environmental influence across grain types and solely analyze disentanglement. As predicted, more complex grains exhibit greater entanglement strength, showing less tendency to disentangle. Interestingly, despite their looser packing, complex grains display a stronger propensity to stay entangled. This observation enables us to establish a nonlinear relationship between the packing fraction of granular media and their flux (escape rate normalized by funnel area), which shows that grains with lower packing fractions exhibit reduced flux (lower disentanglement).

In the next set of experiments (see Figure 3), we examined the entangled interactions between grains and a secondary cluster of elongated objects. By controlling the grains' geometric complexity and quantity, we demonstrated that varying levels of entanglement can be achieved between grains and targets. This enables us to predict the number of entangled interactions within a stochastic system, with a certain level of confidence. Building on these findings, we developed a robotic grasping method that leverages entanglement between grains and targets as the mechanism for picking (Figure 4). The results indicate that grains with greater geometric complexity have a higher propensity to entangle with targets. By linking these results to earlier findings, we conclude that grains exhibiting higher levels of self-entanglement also display stronger entanglement levels during interactions with other clusters.

Lastly, we qualitatively demonstrate several robotic grasping applications by successfully picking various tangle-prone objects (Figure 5A,B). The results show a high success rate for all objects when utilizing grains with greater geometric complexity. Additionally, we leverage this capability to sort tangle-prone objects from non-tangle-prone ones, highlighting another potential application for this grasping approach (Figure 5C). Furthermore, we demonstrate decomposable grains that allow us to separate them from the picked targets (Figure 5D–F). Nevertheless, there are some limitations with the current design of decomposable grains as they need i) to be dropped in water in the case of ferromagnetic dismantlable grains and ii) to be removed from the magnet during each picking iteration in the case of ferromagnetic ice grains.

This study focused on the number of corners as a measure of geometrical complexity, leaving other significant features unexplored. Future research could examine the curvature and the stiffness of the segments that constitute the grains, which may provide deeper insights into their entanglement behavior. Additionally, while this study was solely focused on 2D grains, 3D grains can also be explored, potentially revealing unique patterns and interactions in their entanglement dynamics. Moreover, while the scalability of granular packing was investigated by varying the container size, similar scalability analyses in the context of entangled picking remain unexplored. For instance, studying the relationship between the aspect ratio of target spikes and grain segments could uncover other factors that influence entangled interactions during picking processes. Such studies could also incorporate targets with increasingly complex topologies (e.g., varying thickness, spike configuration, 3D targets).

Furthermore, our robotic picking approach faces several challenges and is presented only as a proof of concept within the context of this research. We acknowledge that the system will require further optimization before it can be implemented in a full industrial setting. One key limitation is the slow operation speed, as the grains must be picked and deployed before the next pick. To enhance efficiency in future designs, we can reduce deployment time by integrating a grain dispenser adjacent to the electromagnet. Additionally, while using an electromagnet with commercially available robotic arms is straightforward at small scales, larger-scale applications could pose significant risks. When substantially larger electromagnets are employed, they may inadvertently damage delicate targets during the picking process. Further studies are needed to assess the feasibility of our picking approach and optimize it for practical implementation at larger scales.

In summary, this study highlights the importance of geometric complexity in governing the entangled interactions within granular metamaterials, both in clustered configurations and during robotic grasping applications. By demonstrating the strong correlation between a grain's structural features and its propensity for entanglement, we provide valuable insights into the design and optimization of such materials. Furthermore, the novel grasping method utilizing entangled interactions opens new avenues for tackling challenges in robotic manipulation, particularly for tangle-prone objects. While this study lays the groundwork for understanding entanglement dynamics, further exploration of other geometrical factors and scalability aspects will be essential to fully unlock the potential of entangled granular metamaterials.

4. Experimental Section

Refer to the Supporting Information for the details of the methods and manufacturing of the grain fabrication, granular simulation, and robotic picking experiment.

Supporting Information

Supporting Information is available from the Wiley Online Library or from the author.

Acknowledgements

The authors would like to thank the technician team at King's College London: Charlotte Plamer, Samual Piper, Jon West, and Alejandro Ramirez Mancebo, who supported this research with their knowledge and time. Furthermore, the authors would like to thank Barakat Ibrahim Barakat and Yuxuan Wang who helped with fabrication, videography, and post-processing of images taken from the experiments. Additionally, the authors are grateful to the UK Materials and Molecular Modelling Hub for computational resources, which is partially funded by EPSRC (EP/T022213/1, EP/W032260/1 and EP/P020194/1). Lastly, the authors would like to acknowledge the financial support of UK research and innovation: UKRI grant EP/X525571/1 (A.E.F), UKRI grant MR/X035506/1 (A.E.F).

Conflict of Interest

The authors declare no conflict of interest.

Data Availability Statement

The data that support the findings of this study are available from the corresponding author upon reasonable request.

Keywords

clustered objects, collective behavior, entangled granular metamaterials, robotic manipulation, stochastic interactions

Received: July 3, 2025
Published online:

[1] H. Kocharyan, N. Karanjgaokar, *Extreme Mech Lett* **2023**, *58*, 101943.
[2] K. Fu, Z. Zhao, L. Jin, *Adv. Funct. Mater.* **2019**, *29*, 1901258.
[3] E. Brown, N. Rodenberg, J. Amend, A. Mozeika, E. Steltz, M. R. Zakin, H. Lipson, H. M. Jaeger, *Proc. Natl. Acad. Sci. USA* **2010**, *107*, 18809.
[4] J. M. Bajkowski, B. Dyniewicz, C. I. Bajer, *Mech Syst Signal Process* **2016**, *70*, 387.
[5] M. Trepanier, S. V. Franklin, *Phys. Rev.* **2010**, *82*, 011308.
[6] K. Desmond, S. V. Franklin, *Phys. Rev. E* **2006**, *73*, 031306.
[7] D. Markauskas, R. Kačianauskas, A. Džiugys, R. Navakas, *Granular Matter* **2009**, *12*, 107.
[8] M. Hansell, *Bird Nests and Construction Behaviour*, Cambridge University Press, Cambridge, England **2000**.
[9] K. Bertoldi, V. Vitelli, J. Christensen, M. Hecke, *Nature Reviews* **2017**, *2*, 17066.
[10] E. Barchiesi, M. Spagnuolo, L. Placidi, *Mathematics and Mechanics of Solids* **2018**, *24*, 212.
[11] M. F. Ashby, R. F. M. Medalist, *Metallurgical Transactions A* **1983**, *14*, 1755.
[12] X. Xia, C. M. Spadaccini, J. R. Greer, *Nat. Rev. Mater.* **2022**, *7*, 683.
[13] A. Elia Forte, D. Melancon, M. Zanati, M. De Giorgi, K. Bertoldi, *Adv. Funct. Mater.* **2023**, *33*, 2214897.
[14] M. C. Fernandes, S. Mhatre, A. E. Forte, B. Zhao, O. Mesa, J. C. Weaver, M. Bechthold, K. Bertoldi, *Extreme Mechanics Letters* **2022**, *51*, 101549.
[15] Y. Yang, A. Vallecchi, E. Shamonina, C. J. Stevens, Y. Zhang, *Sci. Rep.* **2023**, *13*, 1219.
[16] G. Bordiga, E. Medina, S. Jafarzadeh, C. Bösch, R. P. Adams, V. Tournat, K. Bertoldi, *Nat. Mater.* **2024**, *23*, 1486.
[17] L. Jin, A. E. Forte, B. Deng, A. Rafsanjani, K. Bertoldi, *Adv. Mater.* **2020**, *32*, 2001863.
[18] Y. Yang, K. Vella, D. P. Holmes, *Sci. Rob.* **2021**, *6*, abd6426.
[19] A. Lamoureux, K. Lee, M. Shlian, S. R. Forrest, M. Shtein, *Nat. Commun.* **2015**, *6*, 8092.
[20] M. Zaiser, S. Zapperi, *Nat. Rev. Phys.* **2023**, *5*, 679.
[21] H. Gao, in *Advances in Fracture Research*, (Eds.: A. Carpinteri, Y. Mai, R. O. Ritchie), Springer, Netherlands, Dordrecht **2006**, pp. 101.
[22] N. Reznikov, M. Bilton, L. Lari, M. M. Stevens, R. Kröger, *Science* **2018**, *360*, 6388.
[23] M. E. Launey, R. O. Ritchie, *Adv. Mater.* **2009**, *21*, 2103.
[24] D. Haver, D. Acuña, S. Janbaz, E. Lerner, G. Düring, C. Coulais, *Proc Natl Acad Sci U S A* **2024**, *121*, 2317915121.
[25] Z. Meng, H. Yan, Y. Wang, *Sci. Adv.* **2024**, *10*, 49.
[26] J. Zhao, S. Zhao, S. Luding, *Nat. Rev. Phys.* **2023**, *5*, 505.
[27] D. P. Huet, M. Jalaal, R. Beek, A. W. van, *Physical Review Fluids* **2021**, *6*, 104304.
[28] K. Dierichs, A. Menges, *Bioinspir. Biomim.* **2021**, *16*, 065010.
[29] N. Gravish, S. V. Franklin, D. L. Hu, D. I. Goldman, *Phys. Rev. Lett.* **2012**, *108*, 208001.

[30] K. Becker, C. Teeple, N. Charles, Y. Jung, D. Baum, J. C. Weaver, L. Mahadevan, R. Wood, *Proc. Natl. Acad. Sci. USA* **2022**, *119*, 2209819119.
[31] G. Kang, Y.-J. Kim, S.-J. Lee, S. K. Kim, D.-Y. Lee, K. Song, *Nat. Commun.* **2023**, *14*, 4633.
[32] G. J. Monkman, S. Hesse, R. Steinmann, H. Schunk, *Robot Grippers*, John Wiley & Sons, Hoboken, New Jersey, US **2007**.
[33] G. Leão, C. M. Costa, A. Sousa, G. Veiga, *Appl. Sci.* **2020**, *10*, 2264.
[34] X. Zhang, Y. Domae, W. Wan, K. Harada, *Robotic Bin Picking for Potentially Tangled Objects*, Springer International Publishing, Heidelberg, Germany **2024**, pp: 103.
[35] K. Takahashi, N. Fukaya, A. Ummadisingu, *IEEE Robot Autom Lett* **2022**, *7*, 1222.
[36] P. Ray, M. J. Howard, *2020 IEEE/RSJ International Conf. on Intelligent Robots and Systems (IROS)*, Las Vegas, NV, USA, October **2020**.
[37] Y. Sohn, S. Pezeshki, F. Barthelat, *Granular Matter* **2025**, *27*, 55.
[38] A. P. Thompson, H. M. Aktulga, R. Berger, D. S. Bolintineanu, W. M. Brown, P. S. Crozier, P. J. in 't Veld, A. Kohlmeyer, S. G. Moore, T. D. Nguyen, R. Shan, M. J. Stevens, J. Tranchida, C. Trott, S. J. Plimpton, *Comput. Phys. Commun.* **2022**, *271*, 108171.
[39] A. Rezanejad, M. Mousa, M. Howard, A. E. Forte, arXiv **2024**, https://doi.org/10.48550/arXiv.2407.17840.